

Analysis of Photocatalytic Nitrogen Fixation on Rutile $\text{TiO}_2(110)$

Benjamin M. Comer and Andrew J. Medford*

*School of Chemical & Biomolecular Engineering, Georgia Institute of Technology, Atlanta,
GA, 30318*

E-mail: andrew.medford@chbe.gatech.edu

Phone: +1 (404) 385-5531

Abstract

Photocatalytic nitrogen fixation provides a promising route to produce reactive nitrogen compounds at benign conditions. Titania has been reported as an active photocatalyst for reduction of dinitrogen to ammonia; however there is little fundamental understanding of how this process occurs. In this work the rutile (110) model surface is hypothesized to be the active site, and a computational model based on the BEEF-vdW functional and computational hydrogen electrode is applied in order to analyze the expected dinitrogen coverage at the surface as well as the overpotentials for electrochemical reduction and oxidation. The results indicate that the thermodynamic limiting potential for nitrogen reduction on rutile (110) is considerably higher than the conduction band edge of rutile TiO_2 , even at oxygen vacancies and iron substitutions, indicating that this is unlikely to be the relevant surface for nitrogen reduction. However, the limiting potential for nitrogen oxidation on rutile (110) is significantly lower, indicating that oxidative pathways may be relevant on rutile (110). These findings suggest that photocatalytic dinitrogen fixation may occur via a complex balance of oxidative and reductive processes.

Keywords

density functional theory, uncertainty analysis, nitrogen reduction, nitrogen oxidation, nitrogen fixation

Introduction

The Haber-Bosch process enabled synthetic ammonia production at industrial scales, leading to an increased availability of fertilizer that changed the course of human history.^{1,2} However, the process requires a fossil-fuel-derived hydrogen feedstock and high temperatures/pressures, necessitating significant energy resources and centralized production.³ A process for nitrogen fixation that occurs at near-ambient conditions without a hydrogen feedstock will have a transformational impact on global agricultural practices by enabling distributed, sustainable fertilizer production.^{4,5} Photo(electro)chemical nitrogen fixation is a particularly attractive route for producing fertilizers since the electrical driving force can be obtained through renewable energy and delivered at ambient conditions.⁶ In addition, photocatalytic nitrogen fixation has been proposed to occur on natural materials,^{7,8} suggesting that it may influence the natural nitrogen cycle.^{8,9} The anthropological and ecological significance of photocatalytic nitrogen fixation indicate the importance of understanding the conditions and catalytic materials that enable it.

The photocatalytic reduction of atmospheric nitrogen was first proposed in the soil science community,⁷ and was later demonstrated under photocatalytic conditions by Schrauzer and Guth.^{8,10} These efforts spurred numerous studies on photocatalytic nitrogen fixation by titania catalysts^{11–17} that resulted in a variety of interesting observations. It was shown that dinitrogen can be converted to ammonia under both aqueous conditions^{12,16} and humidified air,^{8,10} with higher rates observed in gas-phase conditions.¹⁴ Further, the titania photocatalysts selectively reduce nitrogen to ammonia in most studies,^{8,10,12–14,16} although some work indicates that oxidation to nitrates occurs,^{11,15} and other authors observed no photocatalytic

nitrogen fixation activity.^{18–21} In addition, the presence of the rutile crystal phase and iron dopants were found to be critical for enhancing nitrogen reduction activity.^{8,10,12,13} The iron dopants have been proposed to promote the formation of rutile domains,¹⁰ and/or enhance separation of charge carriers by acting as an electron sink;¹³ while the exact role is not known, the prevailing hypothesis is that Fe is not part of the active site based on the observation that excess Fe content reduces catalytic activity.¹³ More recently, the solar-to-ammonia efficiency was measured to be around 0.02% for a pure titania sample, and the authors hypothesize that the reaction occurs via direct N-N bond scission at a rutile (110) O-br active site.¹⁶ Despite the long history of photocatalytic nitrogen fixation on titania catalysts and numerous experimental results, there is little fundamental understanding of the molecular-scale processes that underly this important and potentially transformative photocatalytic process. In this work we investigate the hypothesis that rutile (110) (Figure 1) is the active surface for photocatalytic nitrogen fixation by examining the pristine rutile (110) surface, the defected (110) surface containing an oxygen vacancy, an iron substitution at the (110) surface, and oxidative processes on the pristine (110) surface.

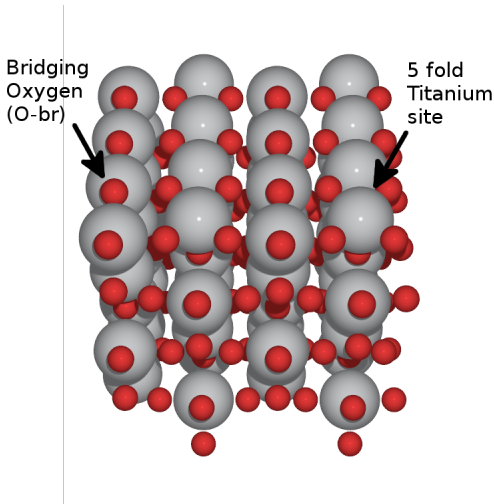


Figure 1: Illustration of TiO_2 (110)

The rutile TiO_2 (110) surface has been well-studied both experimentally^{22–27} and computationally;^{28–31} however, there have been relatively few computational studies of the interac-

tions of rutile TiO_2 surfaces with nitrogen-containing compounds.^{28–30} Two comprehensive computational studies on nitrogen oxides were performed by Stodt et al.²⁸ and Sorescu et al.²⁹ These studies examined N_xO_y compounds on TiO_2 (110) surfaces both experimentally under UHV conditions and theoretically using DFT at the GGA²⁹ and hybrid²⁸ levels of theory. This work showed that DFT is able to accurately obtain the vibrational frequencies of intermediates on the surface and is consistent with UHV experiments. In addition, Cheng et al.³⁰ examined the adsorption of NH_3 (ammonia), NH_2 , and H on clean rutile (110) surfaces using DFT. They concluded that NH_3 and NH_2 adsorb at the 5 fold titanium site whereas hydrogen could bind at the bridging oxygens or the in plane oxygen atoms. Several studies of the binding of ammonia and other nitrogen-containing species have also been investigated for anatase^{32–36} and monoclinic³⁷ polymorphs of TiO_2 .

In contrast to the relatively low number of computational studies there have been many experimental studies of nitrogen compounds on rutile surfaces. Yates and colleagues conducted several studies of NO_x molecules under ultra high vacuum (UHV) conditions over rutile TiO_2 (110).^{24–26} Their early work showed that NO adsorbs and decomposes to form N_2O on reduced surfaces,²⁴ and a follow up study involved photochemical activation of NO on the surface that resulted in the production of N_2O , even with photon energies below the band gap.²⁵ When the surface is dosed with N_2O and exposed to photons at high coverage, N_2O is desorbed from the surface, while at low coverages N_2 is observed.²⁶ Much of this was also seen in the recent examination by Kim and colleagues with the additional insight that surface oxygen vacancies play an important role.^{38,39} Furthermore, numerous applied studies focusing on nitrogen doped titania,⁴⁰ TiO_2 as an ammonia sensor^{41,42} or in the selective catalytic reduction (SCR) process^{43–46} provide insight into the interaction of titania with nitrogen-containing compounds. Although TiO_2 is typically not considered to be the active phase for the SCR reaction,⁴⁷ it is interesting to note a small body of work on the “photo-SCR” where anatase TiO_2 has been proposed as an active and selective catalyst.^{36,48–54} These studies provide useful context for the photocatalytic nitrogen fixation as they involve the

interaction of both oxidized and reduced nitrogen species with titania surfaces.

In addition to nitrogen chemistry, the interaction of titania surfaces with water will play a role in aqueous or humidified environments. Water adsorption on TiO_2 is a topic of extensive research and debate,^{22,55–63} and there are a great variety of theoretical results regarding the competition between dissociative^{60,63} and molecular adsorption^{61,62,64} on pristine surfaces, although a clear consensus has not emerged. Analyses including the effects of slab thickness⁵⁶ and method⁵⁷ support the two modes being nearly degenerate at monolayer coverages, with partial dissociation having a slightly higher energy. This viewpoint is consistent with recent experimental studies observing dissociated water on pristine surfaces.²³ Experimental studies from the mid 1990’s to the mid 2000’s show that on a reduced surface (one containing vacancies at the bridging oxygens) water tends to dissociate to form two hydroxyl groups on the surface, thereby filling the vacancy,^{62,65–67} while on a pristine surface water adsorbs molecularly at the 5-fold Ti site.⁶⁸ As previously noted however, there has been one recent report showing partial dissociation of water on the pristine surface.²³

Several other factors have been observed to play an important role in aqueous TiO_2 photochemistry. The formation of hydroxyl radicals is known to occur in both rutile and anatase,^{69,70} and these radicals participate in a number of oxidation reactions.⁶⁹ Furthermore, the influence of both surface and bulk defects such as oxygen vacancies can enhance adsorption and influence photocatalytic activity.⁷¹ The field of TiO_2 photocatalysis and surface science is vast, and a thorough review is beyond the scope of this work; the reader is referred to published reports and review articles to gain a more complete view.^{22,27,58,59,72}

In this work we present an initial computational investigation of photocatalytic nitrogen reduction and oxidation on the rutile $\text{TiO}_2(110)$ surface. The availability of adsorbed nitrogen is investigated under aqueous and gas-phase conditions, and the thermodynamic stability of adsorbed intermediates for nitrogen reduction and oxidation are investigated. We utilize ab initio thermodynamics^{73,74} and the simple but effective “computational hydrogen electrode” (CHE) approach⁷⁵ that has proven useful in understanding the oxygen

reduction,⁷⁶ oxygen evolution,⁷⁷ CO₂ reduction,⁷⁸ and nitrogen reduction⁷⁹ reactions. Furthermore, the the BEEF-vdW error estimation functional is utilized to assess the robustness of the conclusions. The results indicate that nitrogen adsorption is more favorable under gas-phase conditions, providing a simple explanation for the improved experimental performance. However, the computational evidence refutes the hypothesis that the rutile (110) surface is the active site for nitrogen reduction due to the low stability of adsorbed N₂H_x and NH_x compounds at the pristine surface and at oxygen vacancy and Fe-substitution sites. In contrast, computational results indicate that nitrogen oxidation to NO is a thermodynamically viable fixation route on rutile (110), and it is hypothesized that the N-N bond is dissociated through an oxidative process and the NO intermediate is subsequently reduced.

Results and Discussion

The study of photocatalytic nitrogen fixation on TiO₂ is carried out using DFT calculations to provide molecular-scale insight into the thermochemistry of adsorbed intermediate states. Computational investigations of photocatalysis on TiO₂ are difficult due to the complex nature of photocatalytic interfaces^{75,80} and the electronic structure of TiO₂.^{72,81} In this work we utilize simple models to establish the feasibility of various hypotheses. The energetics of adsorbed species are computed under ideal gas-phase conditions (e.g. solvent effects, electric field effects, and coverage effects are neglected) and it is assumed that excitation and charge transport are decoupled from the electrochemical reactions, enabling the use of the CHE approach;^{75,76,78,80} all voltages are relative to CHE (equivalent to RHE) unless otherwise noted. To treat the electronic structure the generalized gradient approximation (GGA) with van der Waals (vdW) level of theory is used. The use of the Bayesian error estimation functional⁸² (BEEF-vdW) provides error estimates that quantify uncertainty in order to assess the sensitivity of conclusions to the error due to the GGA approximation; more details are provided in the Methods section. This approach is used to test four hypotheses, as

discussed in the following sections: i) photocatalytic nitrogen fixation rates are greater in the gas phase than the aqueous phase ii) rutile (110) is an active surface for nitrogen reduction iii) oxygen vacancies or Fe substitutions on rutile (110) are active sites for nitrogen reduction iv) rutile (110) is an active surface for nitrogen oxidation and subsequent NO reduction.

Nitrogen adsorption under gas and aqueous environments

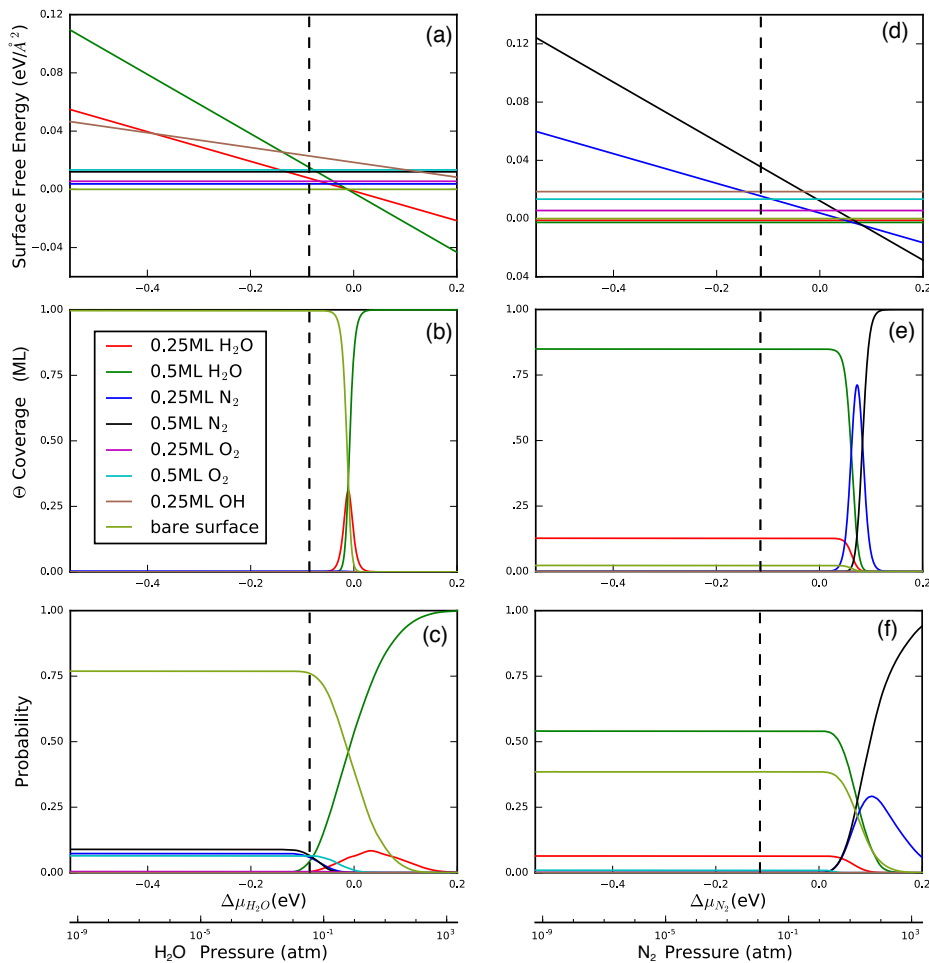


Figure 2: Surface free energy (a,d), coverage (b,e), and coverage probability (c,f) for H₂O, N₂, O₂, and OH as a function of H₂O (a-c) and N₂ (d-f) chemical potentials. The relevant water potential under gas-phase conditions (0.035 atm) and nitrogen potential under aqueous conditions (0.012 atm) are shown by dashed lines in (a-c) and (d-f) respectively. Nitrogen pressure at aqueous conditions is estimated using Henry's law. The probability of various coverages (c,f) given the uncertainty in the BEEF-vdW functional is calculated using Eq. 13.

The literature contains examples of experiments done in aqueous solution^{12,16} and humidified air.^{8,10} Of these, humidified air generally has a higher rate.¹⁴ To better understand the difference in performance under aqueous and gas-phase conditions ab-initio thermodynamics⁷³ have been used to compute surface phase diagrams for rutile (110) as a function of water and nitrogen chemical potentials. Fig. 2a shows the surface free energy (top) and surface coverage (middle) of the reactants available at ambient gas-phase conditions (H_2O , N_2 , O_2 , OH). The results show that the bare TiO_2 surface is dominant at gas-phase conditions. The ensemble of energies from the BEEF-vdW functional can be exploited to evaluate the sensitivity of these coverages to DFT error. The probability analysis (Fig 2a, bottom) suggests that there is a probability of $\approx 10\%$ of having a N_2 coverage > 0.25 ML. One interpretation of this probability is that the BEEF-vdW functional is not sufficiently accurate to precisely determine the surface coverage, though the bare surface is the most likely. Another perspective is to view this as a sensitivity analysis of coverage with respect to binding energies of competing surface species. From this view, the results indicate that adsorption sites with slightly higher relative N_2 adsorption are likely to have a significant N_2 coverage under gas-phase conditions. This could include defect sites or other facets, although the site must have both stronger absolute binding energies and stronger relative adsorption of N_2 vs. H_2O . There are likely sites that satisfy this criterion, but their prevalence must also be considered. Regardless of the interpretation, the conclusion is that nitrogen coverages are expected to be relatively low on rutile TiO_2 (110) which is unsurprising given the inert nature of N_2 .

The surface phase diagrams under aqueous conditions (2b) indicate that water will be the dominant surface species for a wide range of N_2 pressures, with adsorbed N_2 becoming dominant at approximately 100 atm. In this case the probability analysis indicates that although the surface coverage of water is not well-determined by the BEEF-vdW functional, the probability of a significant N_2 coverage is negligible at aqueous conditions. Interestingly, several reports have shown appreciable nitrogen fixation rates under aqueous conditions.^{12,16} The fact that competitive nitrogen adsorption is not favored under aqueous conditions indi-

cates that highly reactive surface groups or defect sites with higher N_2 binding energy but low stability may play a role in aqueous conditions. The finding that nitrogen adsorption is more favorable in the gas phase suggests that the enhanced photocatalytic activity under gas phase conditions is due to the improved ability to adsorb N_2 in the absence of water. This intuitive result corroborates previous findings indicating that a key challenge in photocatalytic nitrogen fixation is getting N_2 to adsorb,^{14,83,84} and qualitatively explains the correlation between N_2 pressure and photocatalytic nitrogen reduction activity.^{14,85} The issue of nitrogen adsorption must be addressed in any photo(electro)catalytic system regardless of reaction mechanism, and will be a fundamental problem for low pressure nitrogen fixation processes.

Thermochemistry of nitrogen reduction

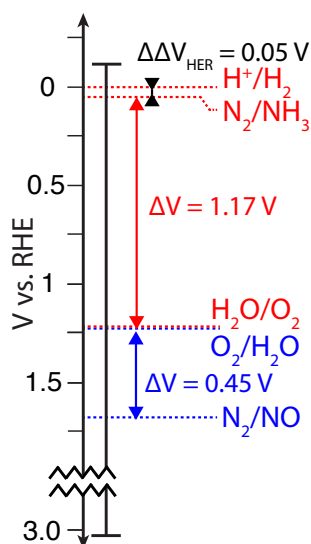


Figure 3: Redox couples for nitrogen reduction (red) and oxidation (blue) with required driving force (ΔV). The difference between hydrogen evolution and nitrogen reduction ($\Delta\Delta V_{\text{HER}}$) is shown to highlight the selectivity challenge for nitrogen reduction. Band edges for rutile TiO_2 are shown (black bar) for reference (note scale break at 1.75 V).

The electrochemical nitrogen reduction reaction converts nitrogen to ammonia and occurs at an equilibrium potential of 0.05 V vs. RHE (Fig. 3). The proximity of this redox couple to the hydrogen evolution reaction (H^+/H_2 at 0 V) makes selective reduction of nitrogen to

ammonia challenging.^{79,86,87} Furthermore, the alignment of the rutile TiO_2 conduction band edge (Fig. 3) indicates that the available overpotential for nitrogen reduction under photocatalytic conditions is relatively low (<0.15 V). Nonetheless, selective nitrogen reduction has been observed on TiO_2 photocatalysts.^{8,10,12,14} This suggests that identification of the active site for photocatalytic nitrogen reduction may enable the development of improved nitrogen reduction electrocatalysts. In this section we hypothesize that the active site is pristine rutile (110), and examine the binding free energies of intermediates for the dissociative and associative nitrogen reduction pathways.

The mechanism for thermocatalytic nitrogen reduction (i.e. Haber-Bosch catalysis) is established as a dissociative mechanism in which the first step is scission of the N-N bond, followed by hydrogenation of adsorbed mono-nitrogen;⁸⁸⁻⁹¹ the electrochemical equivalent is shown in equations 1 - 6. Calculations of N-N scission on rutile oxides shows that they follow “ideal” scaling, suggesting that the activation barrier for nitrogen dissociation may be low,⁹² hence we first investigate the dissociative mechanism. Figure 4 shows the free energy diagram for the dissociative mechanism at standard temperature and pressure at the equilibrium potential. The dissociation energy of N_2 is remarkably high (>8.5 eV), indicating that this route is not remotely thermodynamically feasible on rutile (110). This extreme barrier is not sensitive to the BEEF-vdW XC approximation, and is expected to be prohibitively large even in the presence of solvent stabilization since each adsorbed N^* would need to be stabilized by >3 eV, significantly more than typical solvent stabilization values.^{80,93,94} This provides strong evidence against direct dissociation of the N-N bond on the pristine rutile TiO_2 surface.

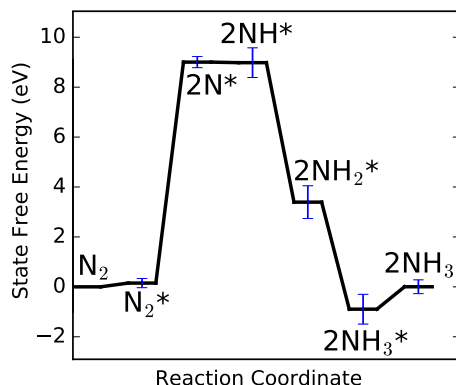
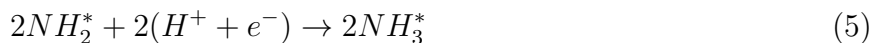
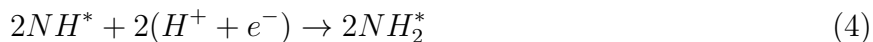
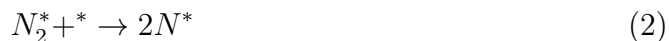


Figure 4: Free energy diagram for dissociative nitrogen reduction at the equilibrium potential computed from DFT (0.008 V, compared to 0.05 V from experiment). The blue error bars represent one standard deviation of the BEEF-vdW energy ensemble. Adsorbed states are labeled, and the full reaction mechanism is listed in equations 1 - 6.

The associative nitrogen reduction mechanism proceeds via diazene (N_2H_2) and hydrazine (N_2H_4), as shown in equations 7 - 12. This mechanism has been proposed to be most relevant for electrochemical nitrogen reduction,^{79,95} and the fact that hydrazine has been observed as a photoreduction product on TiO_2 ¹⁴ suggests that it may be the relevant photocatalytic nitrogen reduction mechanism. The free energy diagram for the associative mechanism at the equilibrium potential is shown in Fig. 5a, while the free energy diagram at the conduction band edge energy for rutile is shown in Fig. 5b. Under photocatalytic conditions the conduction band edge is the relevant potential, corresponding to an overpotential of 0.15 V.

However, examination of the free energy diagram reveals a thermodynamic limiting potential of 2.5 V due to the unstable NNH^* adsorbed intermediate. This barrier is significantly higher than the conduction band potential, making the route improbable unless the adsorbates are stabilized significantly (≈ 2 eV) by solvent/dipole effects. The rate-limiting hydrogenation of N_2 is consistent with studies of electrochemical nitrogen reduction on metals⁷⁹ and nitrides,⁹⁶ indicating a general trend for photo- and electrochemical nitrogen reduction.

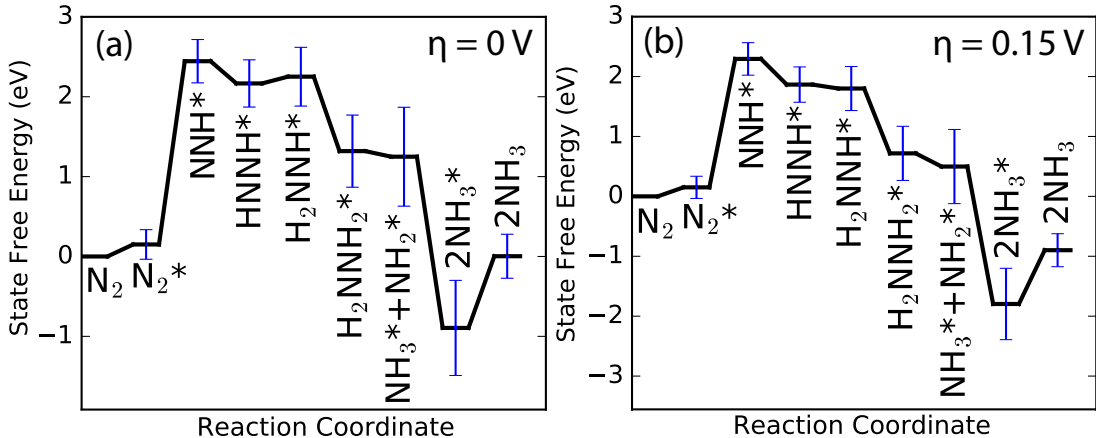


Figure 5: Free energy diagram for associative nitrogen reduction at an overpotential (η) of zero (a) and at the overpotential due to the conduction band edge ($\eta = 0.15$ V) (b). The equilibrium potential ($\eta = 0$) is computed to be 0.008 V (0.05 V experimentally). The blue error bars represent one standard deviation of the BEEF-vdW energy ensemble. Adsorbed states are labeled, and the full reaction mechanism is listed in equations 7 - 12.

The results indicate a prohibitively high barrier for both dissociative and associative

nitrogen reduction on pristine rutile TiO_2 (110), although the associative pathway is significantly more favorable than the dissociative pathway. These findings are robust to the error of the exchange-correlation approximation employed, and the energetic barriers are significantly larger than the typical magnitude of electrochemical interface effects that have been neglected (solvent, electric field). This evidence refutes the hypothesis that rutile (110) is the active site for photocatalytic nitrogen reduction on TiO_2 , necessitating the development and testing of alternative hypotheses.

Nitrogen reduction at oxygen vacancies and iron substitutions

Surface defects are known to play a key role in many types of heterogeneous catalysis,⁹⁷ and oxygen vacancies in particular have been shown to participate in numerous catalytic reactions on oxides⁹⁸ including TiO_2 .^{38,39,58,59,72} Oxygen vacancies are typically highly reactive, leading to binding energies that are often substantially stronger than binding at the stoichiometric surface. The unstable nature of N_2H on pristine rutile (110) (Fig. 5) indicates that defect sites may enable nitrogen reduction by enhancing the stability of N_2H and other high-energy intermediates. Bridging oxygen (O-br) vacancies are known to occur commonly on rutile (110) surfaces,^{58,59,72} and a recent analysis of nitrogen reduction over titania has shown that the reaction rate is proportional to the measured number of bridging oxygen defects.¹⁶ Due to these considerations the O-br vacancy is a natural starting point for evaluating the effect of surface defects, although it is noted that other intrinsic defects, such as Ti vacancies in the surface or sub-surface may also play a role.⁹⁹

The energetics of the associative nitrogen reduction pathway at the rutile (110) O-br defect site are shown in Fig. 6. Comparison to the energetics of the pristine surface (Fig. 8a) reveals a significant stabilization of the N_2H intermediate, corresponding to a thermodynamic limiting potential of 1.21 V. However, examination of the energy diagram at the conduction band potential of rutile TiO_2 (Fig. 6b) indicates that the N_2H and N_2H_2 intermediates are still too unstable to explain the photocatalytic reduction observed, although it

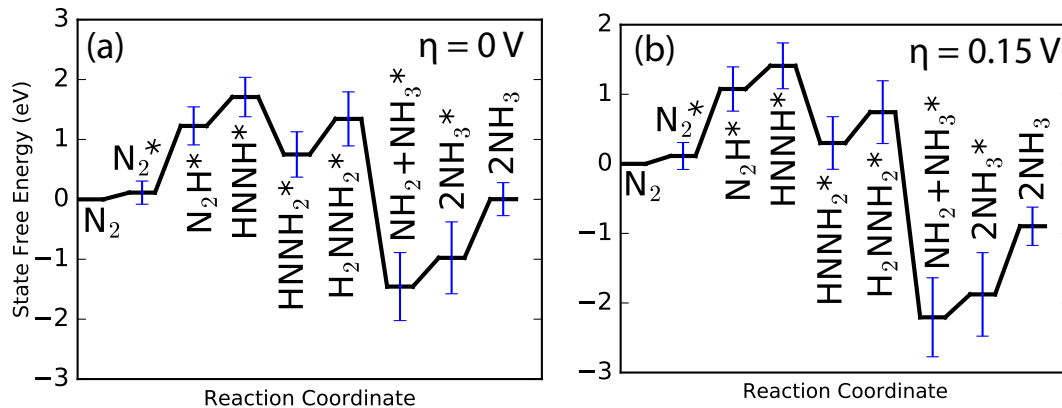


Figure 6: Free energy diagram for associative nitrogen reduction at an O-br vacancy site at an overpotential (η) of zero (a) and at the overpotential due to the conduction band edge ($\eta = 0.15$ V) (b). The equilibrium potential ($\eta = 0$) is computed to be 0.008 V (0.05 V experimentally). The blue error bars represent one standard deviation of the BEEF-vdW energy ensemble. Adsorbed states are labeled, and the full reaction mechanism is listed in the Supporting Information.

is plausible that the thermodynamic barrier of 1.39 eV (energy of N_2H_2 at the conduction band edge) may be overcome by stabilization if solvent or dipole effects for N_2H and N_2H_2 are considerably larger than typical amounts of ≈ 0.6 eV.^{80,93,94} Furthermore, other defects such as sub-surface O or Ti vacancies may increase the reactivity of the surface, although as defects become less stable they will also become less prevalent on the surface. This tradeoff between stability and reactivity has been noted previously for amorphous oxides,¹⁰⁰ and suggests that more reactive (unstable) defects will have a limited impact due to low prevalence. The O-br defect considered here has a formation free energy of 1.54 eV at 0V SHE referenced against water, indicating that it will occur with an relatively low probability on thermodynamically equilibrated surfaces. Morphological (e.g. particle edges) and kinetic (e.g. trapped bulk defects) effects will increase the prevalence of vacancies or other defects in real catalysts;⁷¹ these effects are difficult to control and characterize, and may be the source of some discrepancies in the nitrogen photofixation literature.¹⁷

In addition, many experimental studies have noted that iron dopants significantly increase the nitrogen photofixation rates.^{8,10,12,13} Iron dopants may affect catalyst activity through

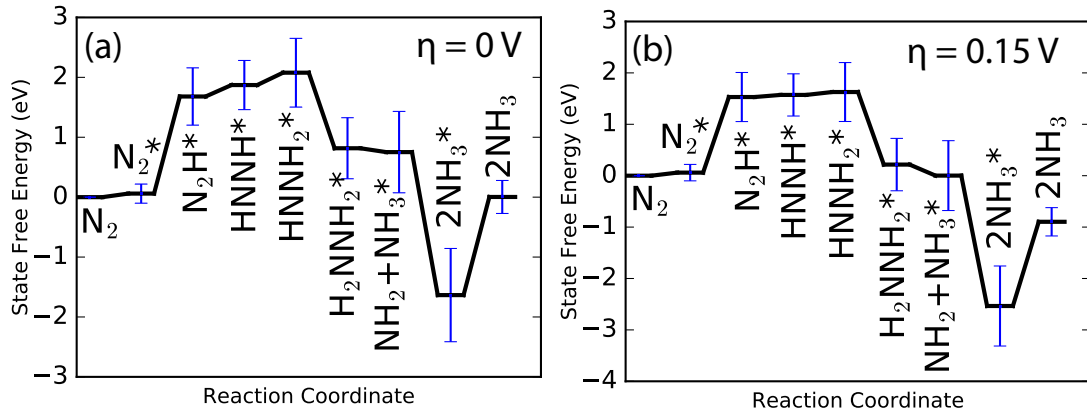


Figure 7: Free energy diagram for associative nitrogen reduction at an iron substitution site at an overpotential (η) of zero (a) and at the overpotential due to the conduction band edge ($\eta = 0.15\text{ V}$) (b). The equilibrium potential ($\eta = 0$) is computed to be 0.008 V (0.05 V experimentally). The blue error bars represent one standard deviation of the BEEF-vdW energy ensemble. Adsorbed states are labeled, and the full reaction mechanism is listed in the Supporting Information.

effects in the bulk or on the surface chemistry. In the bulk, iron has been shown to improve charge separation, reducing recombination of electron-hole pairs. This charge separation enhancement has been suggested to be the dominant effect of iron dopants for photocatalytic nitrogen fixation on titania.¹³ Alternatively, an iron substitution at the surface may stabilize the states along the reductive pathway, directly improving the energetics of the process. The latter hypothesis was tested by substituting the 5-fold titanium with an iron atom and repeating the analysis. Fig. 7 shows the energetics of the associative pathway with an iron-substituted rutile (110) surface. The limiting potential is comparable to that of the defected surface in Fig. 6 ($\approx 1.7\text{V}$). This supports the hypothesis of Soria et al.¹³ that the primary role of iron is to promote charge separation in the bulk structure. The energy required to form this defect was calculated to be 2 eV relative to bulk rutile and BCC iron. The energetic penalty of creating this surface site is high and the improvement to the stability of surface intermediates is moderate, indicating this is unlikely to be an active site for nitrogen reduction. The energetics of the associative pathway on Fe-substitution defects is compared to O-br defects and pristine rutile (110) in Fig. 8a, illustrating that the Fe-substitution

defect has a significantly smaller effect than the O-br vacancy.

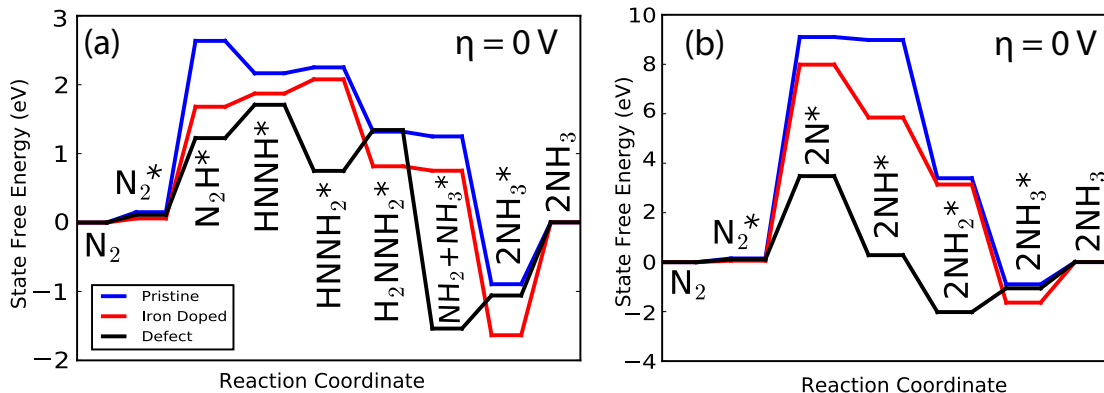


Figure 8: Comparison of free energy pathways over pristine (blue), iron-doped (red) and oxygen-vacancy defect (black) for the associative (a) and dissociative (b) nitrogen reduction pathways at the equilibrium potential. All details are consistent with Figs. 4a - 7a. Error bars are omitted for clarity.

Another possibility is that O-br vacancies and/or Fe-substitution defects significantly impact the energetics of the dissociative pathway. Iron catalysts are known to activate the N-N bond in the Haber-Bosch process,^{88,91} suggesting that the Fe site may play a role, and Hirakawa et. al.¹⁶ have hypothesized that direct N-N bond scission at O-br vacancies is the mechanism for photocatalytic nitrogen fixation. The energetics of the dissociative pathway for both Fe-substitution and O-br vacancy defects are compared with the energetics of the pristine surface in Fig. 8b. The results show that the Fe-substitution has a relatively small effect on the thermodynamics of N-N bond scission, although a more pronounced effect is seen for NH^* intermediates that are stabilized by >1 eV. The O-br vacancies have a much larger effect on N-N bond scission, stabilizing adsorbed N^* by >2 eV per adsorbate. However, the thermodynamic barrier of ≈ 4 eV is still prohibitive at ambient conditions, and significantly higher than the 1.21 V thermodynamic limiting potential needed for the associative mechanism at the O-br vacancy. Furthermore, we note that the free energy diagram in Fig. 8b requires two O-br vacancies, since each N^* is adsorbed at a vacancy. The relatively high formation energy of O-br vacancies suggests that this is improbable, and the experimental investigation of Hirakawa et. al.¹⁶ shows a linear dependence on oxygen

vacancies, rather than the quadratic dependence that would be indicative of direct N-N scission. This finding strongly refutes the proposed hypothesis that direct N-N scission by O-br vacancies is the mechanism of photocatalytic nitrogen fixation on TiO₂. However, the fact that the O-br vacancy significantly stabilizes NH_x species, making NH_x binding close to exothermic suggests that it can promote nitrogen reduction and ammonia formation after the N-N bond has been cleaved.

Nitrogen oxidation and indirect reduction

The majority of experimental investigations of photocatalytic nitrogen fixation on TiO₂ catalysts have identified reduced products of ammonia or ammonium. However, several reports have observed nitrates as the main product,^{11,15} and examination of the standard redox potentials and TiO₂ band edges (3) indicates that the band alignment for nitrogen oxidation to NO is significantly more favorable on TiO₂ than the band alignment for nitrogen reduction. The band alignment provides ≈ 1.3 V overpotential for both the oxygen reduction half-reaction, and the oxidation of nitrogen for NO. Based on this we hypothesize that the scission of the N-N bond on rutile (110) proceeds via the oxidation of nitrogen to NO, which is subsequently oxidized or reduced depending on the details of the catalyst and reaction conditions.

The thermodynamics of nitrogen oxidation intermediates on rutile (110) are shown in Fig. 9 at the equilibrium potential (a) and the energy of the TiO₂ valence band edge (b). Examination of the free energy profile at the equilibrium potential (Fig. 9a) reveals that the thermodynamic limiting potential is 0.72 V (surface oxygen formation is the potential-limiting step), considerably lower than the case of nitrogen reduction. When the significant driving force provided by the photo-excited hole (1.22 V overpotential) is taken into account (Fig. 9b) the oxidative path becomes extremely favorable, with the highest energy state being adsorbed N₂. We note that this analysis considers only the thermodynamics of adsorbed states, and neglects activation barriers that will ultimately govern the kinetics of the process.

These barriers could potentially be significant for N-O coupling, although the strong driving force under photocatalytic conditions will improve the kinetics of any electrochemical step.

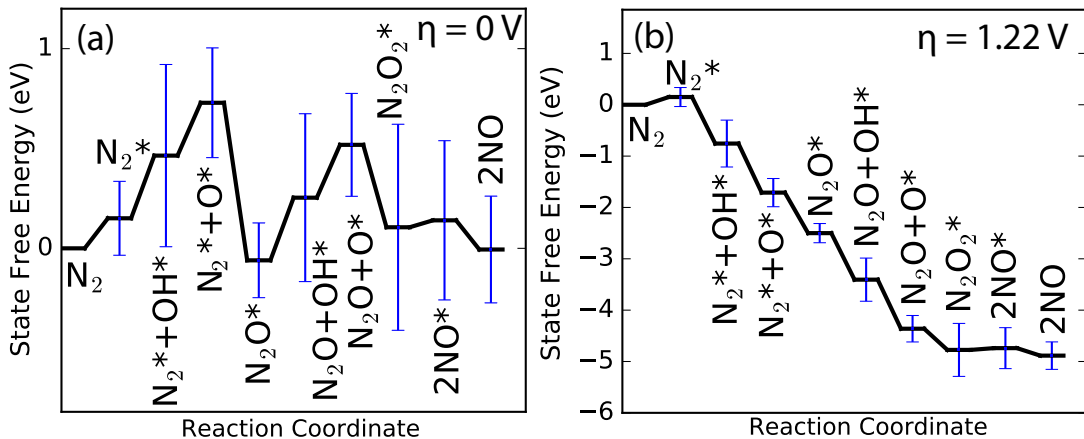


Figure 9: Free energy diagram for nitrogen oxidation to NO at an overpotential (η) of zero (a) and at the overpotential due to the conduction band edge ($\eta = 1.22$ V) (b). The equilibrium potential ($\eta = 0$) is computed to be 1.465 V (1.68 V experimentally). The blue error bars represent one standard deviation of the BEEF-vdW energy ensemble. Adsorbed states are labeled, and the full reaction mechanism is listed in the Supporting Information.

The computational results provide strong evidence that nitrogen oxidation is thermodynamically favored on the rutile (110) active site, which is at odds with the experimental observation of reduced products on TiO_2 ^{8,10,12–14,16} One possible explanation is that nitrogen is first oxidized to NO and subsequently reduced to ammonia. The conversion of NO to NH_3 is a 5 electron process with a redox potential at 0.71 V vs. RHE, well below the band gap of TiO_2 .¹⁷ Titania photocatalysts have been reported to reduce nitrates under aqueous conditions, although selectivity to dinitrogen vs. ammonia varies widely based on preparation conditions and metal dopants.^{101–106} Contrarily, oxidation of ammonia has also been reported for TiO_2 photocatalysts,^{107–109} as well as simultaneous reduction of nitrate and oxidation of ammonium to N_2 .¹⁰⁹ Furthermore, the observation of hydrazine as a product from TiO_2 nitrogen photofixation is not explained by this mechanism.¹⁴ These conflicting results suggest that other hypotheses should also be considered. In particular, the formation of hydrazine should be examined more closely to determine if hydrazine could be formed through recombination of NH_x species (consistent with the oxidative pathway) or if it is

formed associatively (consistent with the reductive pathway). Isotopic scrambling experiments¹¹⁰ and use of photoelectrochemical applied bias experiments may provide insight into this outstanding question.

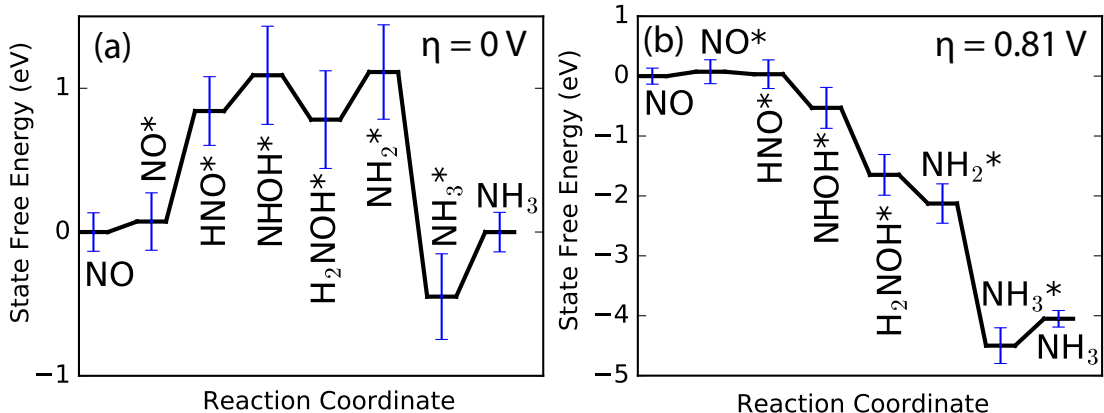


Figure 10: Free energy diagram for NO reduction to NH_3 at an overpotential (η) of zero (a) and at the overpotential due to the conduction band edge ($\eta = 0.81$ V) (b). The equilibrium potential ($\eta = 0$) is computed to be 0.59 V (0.71 V experimentally). The blue error bars represent one standard deviation of the BEEF-vdW energy ensemble. Adsorbed states are labeled, and the full reaction mechanism is listed in the Supporting Information.

Conclusions

The hypothesis that any of the sites on pristine rutile (110) are the active site for nitrogen reduction was shown to be false based on the results of BEEF-vdW DFT calculations for both the associative and dissociative mechanism, although the associative mechanism was found to be considerably more thermodynamically favorable. The revised hypothesis that oxygen vacancies or Fe substitutions are active sites was shown to be more plausible, and a significant stabilization of NH_x by O-br vacancies was found. Yet, the predicted thermodynamic barriers are considerably higher than the conduction band edge, and the defects are not predicted to be thermodynamically stable under operating conditions, leading to the conclusion that this hypothesis is also improbable. However, the results indicate that N-N bond cleavage is thermodynamically facile on rutile (110) through an oxidative pathway, particularly with the

strong oxidative driving force provided by photogenerated holes. Based on this finding, the hypothesis of an oxidized NO* intermediate in nitrogen reduction is introduced as a possible mechanism for photocatalytic nitrogen fixation on rutile (110). The work provides initial molecular-scale insight into the mechanisms that underly photocatalytic nitrogen fixation on TiO₂ by conclusively eliminating several possible explanations for this important process and identifying a novel hypothesis of indirect reduction through an oxidized intermediate.

Methods

Computational

Density Functional Theory

In the current work the Quantum ESPRESSO software package¹¹¹ is used in conjunction with the Atomic Simulation Package (ASE)¹¹² to carry out plane wave density functional theory calculations. The BEEF-vdw functional⁸² is used for all work with a plane wave cutoff of 400 eV and a 4x4x1 Monkhorst-Pack k-point grid is used for all slab models.¹¹³ Spin polarization and a dipole correction¹¹⁴ (applied along the axis of the slab) are used for all slab calculations. Structures are optimized using the BFGS line search method to a total force of 0.05 eV/Å. The geometries and adsorption energies for all species are available in Tables S1 and S3. All gas-phase species are evaluated in a periodic unit cell with 6 Å of vacuum space and a Γ -point k-point sampling. A number of calculated properties of TiO₂ (e.g. band gap, water adsorption energy) vary with the number of layers in the model slab,^{55,115,116} slabs with an even number of layers are known to be more accurate due to a symmetric electronic environment between sets of layers.⁵⁵ The error due to slab size is expected to be ca. 0.2 eV,⁵⁵ similar to the error of DFT for adsorption energies.¹¹⁷ Furthermore, there is debate regarding the accuracy of GGA functionals for TiO₂. Several studies have indicated that catalytic properties, even of defects, can be reliably treated with GGA functionals,^{62,118,119} although

other work indicates that hybrid, +U, or double-hybrid methods are necessary, particularly to treat electronic transitions and optical properties.¹²⁰⁻¹²³ In this work we utilize the error estimation capabilities of the BEEF-vdW functional⁸² in order to estimate its accuracy and quantify the uncertainty due to the GGA approximation. Although the quantitative accuracy of BEEF-vdW error estimation in oxide materials is not well-known,¹²⁴ the BEEF-vdW ensembles provide a systematic way to assess the sensitivity of conclusions to accuracy of approximations.¹²⁵ The error bars shown in this work correspond to $\pm 1\sigma$ of the ensemble of 2000 energies provided by the BEEF-vdW functional. The uncertainty quantified in the BEEF ensembles is also propagated to phase diagrams (Fig. 2). The probability of a species on the surface is defined as:

$$P_i = \frac{1}{N} \sum_l^N \frac{\exp(\frac{-G_i^l}{kT})}{\sum_j^M \exp(\frac{-G_j^l}{kT})} \quad (13)$$

where P_i is the probability of species i given DFT uncertainty, G_i^l is the free energy of species i computed from energy l of the BEEF-vdW ensemble, M are the number of total species considered, and N is the total number of energies in the BEEF-vdW ensemble (2000). This is equivalent to the average surface coverage from a ensemble of phase diagrams generated from the energies of the BEEF-vdW ensemble.

Thermochemistry

Ground state electronic energies (E_{ele}) are obtained from DFT and converted to free energies by including zero point energy (ZPE) and thermal contributions:

$$G_i^o = E_{ele} + E_{ZPE} + \Delta H - T\Delta S \quad (14)$$

where E_{ZPE} is the zero-point energy and ΔH (enthalpy) and ΔS (entropy) are thermal contributions computed using the vibrational frequencies computed through a finite difference approximation to the Hessian. Adsorbates are treated using the harmonic approximation

with a low-frequency cutoff of 30 cm^{-1} , while gas phase molecules were treated as ideal gases. The ASE implementation¹¹² is used for vibrational analysis and statistical mechanics corrections. Vibrational frequencies for all species are reported in Table S2. Vibrational frequencies of adsorbates at defect sites are assumed to be the same as vibrational frequencies on the pristine surface. All thermodynamics were evaluated at 300 K and set to their atmospheric values (0.8 atm N_2 , 0.2 atm O_2). Liquid water was approximated as an ideal gas at saturation pressure at 300 K (0.031 atm). Relative (formation) energies were computed with respect to reference states using the equation:

$$G_i = G_i^o - \sum_j n_j \mu_j \quad (15)$$

where G_i is the formation free energy of species i , G_i^o is the “absolute” free energy computed from DFT and free energy corrections (see Equation 14), n_j is the number of atoms j in species i , and μ_j is the reference chemical potential. The reference for nitrogen is N_2 ($\mu_N = \frac{1}{2}G_{\text{N}_2}^o$), the reference for oxygen is O_2 ($\mu_O = \frac{1}{2}G_{\text{O}_2}^o$) and the reference for hydrogen is H_2 ($\mu_H = \frac{1}{2}G_{\text{H}_2}^o$). In this work no gas-phase corrections (e.g. O_2 ,⁷⁶ CO_2 ⁷⁸) are applied since it is difficult to rigorously correct the BEEF-vdW ensembles; we expect that the error bars of the BEEF-vdW error ensemble should compensate for these known inaccuracies of DFT.

Photoelectrochemistry

The photoelectrochemical model used assumes that excitation, charge transport, and charge transfer are decoupled from electrochemistry and is largely consistent with the approach reviewed by Hellman and Wang.⁸⁰ All states involving electrons utilized the CHE model reaction as a reference electrode. This model sets the free energy of reaction hydrogen splitting, reaction 16, to zero at a potential of zero. Referencing potentials this way is known as relative to the computational hydrogen electrode (CHE), and is conceptually equivalent to the reference hydrogen electrode (RHE).⁷⁸

The energy of each state involving the addition of an electron is varied by an energy of eU , where e is the fundamental charge and U is the potential relative to this zero point, at potentials other than zero reaction:



This model was also used to assess the effect of photo-excited electrons and holes. The locations of the band edges were obtained from the literature¹²⁶ and used to set the potentials of the electrons and holes. The potential of holes was set to -0.1V and the potential of excited electrons was set to 2.9V, conserving the experimental value of the band gap at 3 eV.¹²⁷

Determination of adsorption sites

Several adsorption sites were tested for stability for all stable molecular species and adatoms. For most stable molecular species the only viable adsorption site was the 5-fold titanium site; attempts to adsorb species to the bridging oxygen or in plane oxygens either led to desorption or reorientation to the 5-fold titanium site. These findings are in agreement with previous first-principles examinations.^{28,29} Adatoms (N*, O*, H*) were found to have multiple adsorption sites. Oxygen was found to adsorb to the 5-fold titanium site or form a diatomic species at the bridging oxygen site. The latter can be identified as the α -oxygen species reported by Lu.²⁴ Hydrogen adatoms were found to be most stable at the in plane oxygen, and the nitrogen adatom was found to have highest stability over the bridging oxygen. A full list of energies and structures is provided in the Supplementary Information.

Acknowledgement

The authors thank the School of Chemical & Biomolecular Engineering at the Georgia Institute of Technology for providing start-up funding for this work. The authors are also grateful to Marta C. Hatzell for constructive discussions, and Timothy Doane for providing

references regarding photocatalytic nitrogen fixation.

Publication Disclosure

This document is the unedited Author's version of a Submitted Work that has been submitted for publication in ACS Sustainable Chemistry and Engineering, copyright American Chemical Society.

References

1. Smil, V. Detonator of the population explosion. *Nature* **1999**, *400*, 415–415.
2. Galloway, J. N.; Dentener, F. J.; Capone, D. G.; Boyer, E. W.; Howarth, R. W.; Seitzinger, S. P.; Asner, G. P.; Cleveland, C. C.; Green, P. A.; Holland, E. A.; Karl, D. M.; Michaels, A. F.; Porter, J. H.; Townsend, A. R.; Vosmarty, C. J. Nitrogen Cycles: Past Present, and Future. *Biogeochemistry* **2004**, *70*, 153–226.
3. Uekoetter, F.; Smil, V. Enriching the Earth. Fritz Haber, Carl Bosch, and the Transformation of World Food Production. *Environmental History* **2002**, *7*, 532.
4. Allman, A.; Tiffany, D.; Kelley, S.; Daoutidis, P. A framework for ammonia supply chain optimization incorporating conventional and renewable generation. *AIChE Journal* **2017**,
5. Gilbert, N. African agriculture: Dirt poor. *Nature* **2012**, *483*, 525–527.
6. Giddey, S.; Badwal, S.; Kulkarni, A. Review of electrochemical ammonia production technologies and materials. *Int. J. Hydrogen Energy* **2013**, *38*, 14576–14594.
7. Dhar, N.; Seshacharyulu, E.; Biswas, N. New aspects of nitrogen fixation and loss in soils. *Proceedings of the National institute of sciences of India* **1941**, *7*, 115–131.

8. Schrauzer, G. N.; Strampach, N.; Hui, L. N.; Palmer, M. R.; Salehi, J. Nitrogen photoreduction on desert sands under sterile conditions. *Proc. Natl. Acad. Sci. U.S.A.* **1983**, *80*, 3873–3876.
9. Doane, T. A. A survey of photogeochemistry. *Geochemical Transactions* **2017**, *18*.
10. Schrauzer, G.; Guth, T. Photocatalytic reactions. 1. Photolysis of water and photoreduction of nitrogen on titanium dioxide. *J. Am. Chem. Soc.* **1977**, *99*, 7189–7193.
11. Bickley, R. I.; Vishwanathan, V. Photocatalytically induced fixation of molecular nitrogen by near UV radiation. *Nature* **1979**, *280*, 306–308.
12. Augugliaro, V.; Lauricella, A.; Rizzuti, L.; Schiavello, M.; Sclafani, A. Conversion of solar energy to chemical energy by photoassisted processes—I. Preliminary results on ammonia production over doped titanium dioxide catalysts in a fluidized bed reactor. *Int. J. Hydrogen Energy* **1982**, *7*, 845–849.
13. Soria, J.; Conesa, J. C.; Augugliaro, V.; Palmisano, L.; Schiavello, M.; Sclafani, A. Dinitrogen photoreduction to ammonia over titanium dioxide powders doped with ferric ions. *J. Phys. Chem.* **1991**, *95*, 274–282.
14. Schrauzer, G. N. *Energy Efficiency and Renewable Energy Through Nanotechnology*; Springer, 2011; pp 601–623.
15. Yuan, S.-J.; Chen, J.-J.; Lin, Z.-Q.; Li, W.-W.; Sheng, G.-P.; Yu, H.-Q. Nitrate formation from atmospheric nitrogen and oxygen photocatalysed by nano-sized titanium dioxide. *Nat. Commun.* **2013**, *4*.
16. Hirakawa, H.; Hashimoto, M.; Shiraishi, Y.; Hirai, T. Photocatalytic Conversion of Nitrogen to Ammonia with Water on Surface Oxygen Vacancies of Titanium Dioxide. *Journal of the American Chemical Society* **2017**, *139*, 10929–10936.

17. Medford, A. J.; Hatzell, M. C. Photon-Driven Nitrogen Fixation: Current Progress, Thermodynamic Considerations, and Future Outlook. *ACS Catalysis* **2017**, 2624–2643.
18. Edwards, J. G.; Davies, J. A.; Boucher, D. L.; Mennad, A. An Opinion on the Heterogeneous Photoreactions of N₂ with H₂O. *Angew. Chem. Int. Ed.* **1992**, 31, 480–482.
19. Davies, J. A.; Edwards, J. G. Reply: Standards of Demonstration for the Heterogeneous Photoreactions of N₂ with H₂O. *Angew. Chem. Int. Ed.* **1993**, 32, 552–553.
20. Boucher, D. L.; Davies, J. A.; Edwards, J. G.; Mennad, A. An investigation of the putative photosynthesis of ammonia on iron-doped titania and other metal oxides. *Journal of Photochemistry and Photobiology A: Chemistry* **1995**, 88, 53–64.
21. Davies, J. A.; Boucher, D. L.; Edwards, J. G. *Advances in Photochemistry*; John Wiley & Sons, Inc., pp 235–310.
22. Benkoula, S.; Sublemontier, O.; Patanen, M.; Nicolas, C.; Sirotti, F.; Naitabdi, A.; Gaie-Levrel, F.; Antonsson, E.; Aureau, D.; Ouf, F.-X.; Wada, S.-I.; Etcheberry, A.; Ueda, K.; Miron, C. Water adsorption on TiO₂ surfaces probed by soft X-ray spectroscopies: bulk materials vs. isolated nanoparticles. *Scientific Reports* **2015**, 5, 15088.
23. Walle, L. E.; Borg, A.; Uvdal, P.; Sandell, A. Experimental evidence for mixed dissociative and molecular adsorption of water on a rutile TiO₂ (110) surface without oxygen vacancies. *Physical Review B* **2009**, 80, 235436.
24. Lu, G.; Linsebigler, a.; Yates, J. T. Ti³⁺ Defect Sites on TiO₂(110): Production and Chemical Detection of Active Sites. *Journal of Physical Chemistry* **1994**, 98, 11733–11738.
25. Rusu, C. N.; Yates, J. T. Photochemistry of NO Chemisorbed on TiO₂ (110) and TiO₂ Powders. *The journal of physical chemistry. B* **2000**, 104, 1729–1737.

26. Rusu, C. N.; Yates Jr., J. T. N₂O Adsorption and Photochemistry on High Area TiO₂ Powder. *J. Phys. Chem. B* **2001**, *105*, 2596–2603.
27. Henderson, M. A. A surface science perspective on TiO₂ photocatalysis. *Surface Science Reports* **2011**, *66*, 185–297.
28. Stodt, D.; Noei, H.; Hättig, C.; Wang, Y. A combined experimental and computational study on the adsorption and reactions of NO on rutile TiO₂. *Physical chemistry chemical physics : PCCP* **2013**, *15*, 466–72.
29. Sorescu, D.; Rusu, C.; Jr, J. Y. Adsorption of NO on the TiO₂ (110) Surface: An Experimental and Theoretical Study. *The Journal of Physical ...* **2000**, *2*, 4408–4417.
30. Cheng, D.; Lan, J.; Cao, D.; Wang, W. Adsorption and dissociation of ammonia on clean and metal-covered TiO₂ rutile (110) surfaces: A comparative DFT study. *Applied Catalysis B: Environmental* **2011**, *106*, 510–519.
31. Diebold, U. The surface science of titanium dioxide. *Surface Science Reports* **2003**, *48*, 53–229.
32. Onal, I.; Soyer, S.; Senkan, S. Adsorption of water and ammonia on TiO₂-anatase cluster models. *Surface Science* **2006**, *600*, 2457–2469.
33. Erdogan, R.; Ozbek, O.; Onal, I. A periodic DFT study of water and ammonia adsorption on anatase TiO₂ (001) slab. *Surface Science* **2010**, *604*, 1029–1033.
34. Erdogan, R.; Onal, I. An ONIOM and DFT study of water and ammonia adsorption on anatase TiO₂ (001) cluster. *International Journal of Quantum Chemistry* **2011**, *111*, 2149–2159.
35. Markovits, A.; Ahdjoudj, J.; Minot, C. A theoretical analysis of NH₃ adsorption on TiO₂. *Surface Science* **1996**, *365*, 649–661.

36. Ji, Y.; Luo, Y. First-Principles Study on the Mechanism of Photoselective Catalytic Reduction of NO by NH₃ on Anatase TiO₂(101) Surface. *JOURNAL OF PHYSICAL CHEMISTRY C* **2014**, *118*, 6359–6364.
37. jing Guo, X.; Liu, W.; Fang, W.; Cai, L.; Zhu, Y.; Lu, L.; Lu, X. DFT study of coverage-dependent adsorption of NH₃ on TiO₂-B (100) surface. *Physical Chemistry Chemical Physics* **2012**, *14*, 16618.
38. Kim, B.; Dohnálek, Z.; Szanyi, J.; Kay, B. D.; Kim, Y. K. Temperature-programmed desorption study of NO reactions on rutile TiO₂(110)-1x1. *Surface Science* **2016**, *652*, 148–155.
39. Kim, B.; Li, Z.; Kay, B. D.; Dohnálek, Z.; Kim, Y. K. Low-Temperature Desorption of N₂O from NO on Rutile TiO₂ (110)-1 x 1. *The Journal of Physical Chemistry C* **2014**, *118*, 9544–9550.
40. Chen, H.; Nambu, A.; Wen,; Graciani, J.; Zhong,; Hanson, J. C.; Fujita, E.; Rodriguez, J. A. Reaction of NH₃with Titania: N-Doping of the Oxide and TiN Formation. *The Journal of Physical Chemistry C* **2007**, *111*, 1366–1372.
41. Karunagaran, B.; Uthirakumar, P.; Chung, S.; Velumani, S.; Suh, E.-K. TiO₂ thin film gas sensor for monitoring ammonia. *Materials Characterization* **2007**, *58*, 680–684.
42. Suganuma, S.; Murakami, Y.; Ohyama, J.; Torikai, T.; Okumura, K.; Katada, N. Assignments of Bending Vibrations of Ammonia Adsorbed on Surfaces of Metal Oxides. *Catalysis Letters* **2015**, *145*, 1904–1912.
43. Busca, G. Chemical and mechanistic aspects of the selective catalytic reduction of NO_x by ammonia over oxide catalysts: A review. *Applied Catalysis B: Environmental* **1998**, *18*, 1–36.

44. Ramis, G.; Busca, G.; Lorenzelli, V.; Forzatti, P. Fourier transform infrared study of the adsorption and coadsorption of nitric oxide, nitrogen dioxide and ammonia on TiO₂ anatase. *Applied Catalysis* **1990**, *64*, 243–257.
45. Giraud, F.; Geantet, C.; Guilhaume, N.; Gros, S.; Porcheron, L.; Kaniche, M.; Bianchi, D. Experimental Microkinetic Approach of De-NO_x by NH₃ on V₂O₅/WO₃/TiO₂ Catalysts. 1. Individual Heats of Adsorption of Adsorbed NH₃ Species on a Sulfate-Free TiO₂ Support Using Adsorption Isobars. *JOURNAL OF PHYSICAL CHEMISTRY C* **2014**, *118*, 15664–15676.
46. Liu, J.; Meeprasert, J.; Namuangruk, S.; Zha, K.; Li, H.; Huang, L.; Maitarad, P.; Shi, L.; Zhang, D. Facet–Activity Relationship of TiO₂ in Fe₂O₃/TiO₂ Nanocatalysts for Selective Catalytic Reduction of NO with NH₃: In Situ DRIFTS and DFT Studies. *The Journal of Physical Chemistry C* **2017**, *121*, 4970–4979.
47. Topsoe, N.-Y. Mechanism of the Selective Catalytic Reduction of Nitric Oxide by Ammonia Elucidated by in Situ On-Line Fourier Transform Infrared Spectroscopy. *Science* **1994**, *265*, 1217–1219.
48. Tanaka, T.; Teramura, K.; Arakaki, K.; Funabiki, T. Photoassisted NO reduction with NH₃ over TiO₂ photocatalyst. *CHEMICAL COMMUNICATIONS* **2002**, 2742–2743.
49. Teramura, K.; Tanaka, T.; Funabiki, T. EPR study of photoinduced electron transfer between adsorbent and adsorbed species in photo-SCR with NH₃. *CHEMISTRY LETTERS* **2003**, *32*, 1184–1185.
50. Teramura, K.; Tanaka, T.; Yamazoe, S.; Arakaki, K.; Funabiki, T. Kinetic study of photo-SCR with NH₃ over TiO₂. *APPLIED CATALYSIS B-ENVIRONMENTAL* **2004**, *53*, 29–36.
51. Yamazoe, S.; Okumura, T.; Teramura, K.; Tanaka, T. Development of the efficient TiO₂ photocatalyst in photoassisted selective catalytic reduction of NO with NH₃.

- CATALYSIS TODAY* **2006**, *111*, 266–270, 10th Japan-Korea Symposium on Catalysis, Matsue, JAPAN, MAY 10-12, 2005.
52. Yamazoe, S.; Teramura, K.; Hitomi, Y.; Shishido, T.; Tanaka, T. Visible light absorbed NH₂ species derived from NH₃ adsorbed on TiO₂ for photoassisted selective catalytic reduction. *JOURNAL OF PHYSICAL CHEMISTRY C* **2007**, *111*, 14189–14197.
53. Yamamoto, A.; Mizuno, Y.; Teramura, K.; Shishido, T.; Tanaka, T. Effects of reaction temperature on the photocatalytic activity of photo-SCR of NO with NH₃ over a TiO₂ photocatalyst. *CATALYSIS SCIENCE & TECHNOLOGY* **2013**, *3*, 1771–1775.
54. Lasek, J.; Yu, Y.-H.; Wu, J. C. S. Removal of NO_x by photocatalytic processes. *JOURNAL OF PHOTOCHEMISTRY AND PHOTOBIOLOGY C-PHOTOCHEMISTRY REVIEWS* **2013**, *14*, 29–52.
55. Sun, C.; Liu, L.-m.; Selloni, A.; Lu, G. Q. M.; Smith, S. C. Titania-water interactions: a review of theoretical studies. *Journal of Materials Chemistry* **2010**, *20*, 10319.
56. Harris, L. A.; Quong, A. A. Molecular Chemisorption as the Theoretically Preferred Pathway for Water Adsorption on Ideal Rutile TiO₂(110). *Physical Review Letters* 086105.
57. Kumar, N.; Kent, P. R. C.; Wesolowski, D. J.; Kubicki, J. D. Modeling water adsorption on rutile (110) using van der waals density functional and DFT+U methods. *Journal of Physical Chemistry C* **2013**, *117*, 23638–23644.
58. Pang, C. L.; Lindsay, R.; Thornton, G. Chemical reactions on rutile TiO₂(110). *Chemical Society reviews* **2008**, *37*, 2328–2353.
59. Pang, C. L.; Lindsay, R.; Thornton, G. Structure of Clean and Adsorbate-Covered Single-Crystal Rutile TiO₂Surfaces. *Chemical Reviews* **2013**, *113*, 3887–3948.

60. Lindan, P.; Harrison, N.; Holender, J.; Gillan, M. First-principles molecular dynamics simulation of water dissociation on TiO₂ (110). *Chemical Physics Letters* **1996**, *261*, 246–252.
61. Bates, S.; Kresse, G.; Gillan, M. The adsorption and dissociation of ROH molecules on TiO₂(110). *Surface Science* *409*, 336–349.
62. Schaub, R.; Thostrup, P.; Lopez, N.; Lægsgaard, E.; Stensgaard, I.; Nørskov, J. K.; Besenbacher, F. Oxygen Vacancies as Active Sites for Water Dissociation on Rutile TiO₂ (110). *Phys. Rev. Lett.* **2001**, *87*.
63. Lindan, P. J. D.; Zhang, C. Exothermic water dissociation on the rutile-TiO₂(110) surface. *Physical Review B* **2005**, *72*.
64. Kowalski, P. M.; Meyer, B.; Marx, D. Composition, structure, and stability of the rutile-TiO₂(110) surface: Oxygen depletion, hydroxylation, hydrogen migration, and water adsorption. *Physical Review B* **2009**, *79*.
65. Henderson, M. A. An HREELS and TPD study of water on TiO₂(110): the extent of molecular versus dissociative adsorption. *Surface Science* **1996**, *355*, 151–166.
66. Krischok, S.; Höfft, O.; Günster, J.; Stultz, J.; Goodman, D.; Kempter, V. H₂O interaction with bare and Li-precovered TiO₂: studies with electron spectroscopies (MIES and UPS(HeI and II)). *Surface Science* **2001**, *495*, 8–18.
67. Ketteler, G.; Yamamoto, S.; Bluhm, H.; Andersson, K.; Starr, D. E.; Ogletree, D. F.; Ogasawara, H.; Nilsson, A.; Salmeron, M. The Nature of Water Nucleation Sites on TiO₂(110) Surfaces Revealed by Ambient Pressure X-ray Photoelectron Spectroscopy. *The Journal of Physical Chemistry C* **2007**, *111*, 8278–8282.
68. Hugenschmidt, M. B.; Gamble, L.; Campbell, C. T. The interaction of H₂O with a TiO₂(110) surface. *Surface Science* **1994**, *302*, 329–340.

69. Ichi Ishibashi, K.; Fujishima, A.; Watanabe, T.; Hashimoto, K. Quantum yields of active oxidative species formed on TiO₂ photocatalyst. *Journal of Photochemistry and Photobiology A: Chemistry* **2000**, *134*, 139–142.
70. Xiang, Q.; Yu, J.; Wong, P. K. Quantitative characterization of hydroxyl radicals produced by various photocatalysts. *Journal of Colloid and Interface Science* **2011**, *357*, 163–167.
71. Yan, J.; Wu, G.; Guan, N.; Li, L.; Li, Z.; Cao, X. Understanding the effect of surface/bulk defects on the photocatalytic activity of TiO₂: anatase versus rutile. *Physical Chemistry Chemical Physics* **2013**, *15*, 10978.
72. Diebold, U. The surface science of titanium dioxide. *Surface Science Reports* **2003**, *48*.
73. Reuter, K.; Scheffler, M. Composition, structure, and stability of RuO₂(110) as a function of oxygen pressure. *Physical Review B* **2001**, *65*.
74. Reuter, K.; Stampf, C.; Scheffler, M. *Handbook of Materials Modeling*; Springer Nature, 2005; pp 149–194.
75. Calle-Vallejo, F.; Koper, M. T. First-principles computational electrochemistry: Achievements and challenges. *Electrochimica Acta* **2012**, *84*, 3–11.
76. Nørskov, J. K.; Rossmeisl, J.; Logadottir, A.; Lindqvist, L.; Kitchin, J. R.; Bligaard, T.; Jónsson, H. Origin of the Overpotential for Oxygen Reduction at a Fuel-Cell Cathode. *J. Phys. Chem. B* **2004**, *108*, 17886–17892.
77. Man, I. C.; Su, H.-Y.; Calle-Vallejo, F.; Hansen, H. A.; Martínez, J. I.; Inoglu, N. G.; Kitchin, J.; Jaramillo, T. F.; Nørskov, J. K.; Rossmeisl, J. Universality in Oxygen Evolution Electrocatalysis on Oxide Surfaces. *ChemCatChem* **2011**, *3*, 1159–1165.
78. Peterson, A. A.; Abild-Pedersen, F.; Studt, F.; Rossmeisl, J.; Nørskov, J. K. How

- copper catalyzes the electroreduction of carbon dioxide into hydrocarbon fuels. *Energy & Environmental Science* **2010**, *3*, 1311.
79. Skulason, E.; Bligaard, T.; Gudmundsdóttir, S.; Studt, F.; Rossmeisl, J.; Abild-Pedersen, F.; Vegge, T.; Jónsson, H.; Nørskov, J. K. A theoretical evaluation of possible transition metal electro-catalysts for N₂ reduction. *Phys. Chem. Chem. Phys.* **2012**, *14*, 1235–1245.
80. Hellman, A.; Wang, B. First-Principles View on Photoelectrochemistry: Water-Splitting as Case Study. *Inorganics* **2017**, *5*, 37.
81. de Dompablo, M. E. A.; Morales-García, A.; Taravillo, M. DFT+U calculations of crystal lattice, electronic structure, and phase stability under pressure of TiO₂ polymorphs. *The Journal of Chemical Physics* **2011**, *135*, 054503.
82. Wellendorff, J.; Lundgaard, K. T.; Møgelhøj, A.; Petzold, V.; Landis, D. D.; Nørskov, J. K.; Bligaard, T.; Jacobsen, K. W. Density functionals for surface science: Exchange-correlation model development with Bayesian error estimation. *Physical Review B* **2012**, *85*, 235149–235149.
83. Zhu, D.; Zhang, L.; Ruther, R. E.; Hamers, R. J. Photo-illuminated diamond as a solid-state source of solvated electrons in water for nitrogen reduction. *Nature Materials* **2013**, *12*, 836–841.
84. Vettraino, M.; Trudeau, M.; Lo, A. Y. H.; Schurko, R. W.; Antonelli, D. Room-Temperature Ammonia Formation from Dinitrogen on a Reduced Mesoporous Titanium Oxide Surface with Metallic Properties. *Journal of the American Chemical Society* **2002**, *124*, 9567–9573.
85. Ali, M.; Zhou, F.; Chen, K.; Kotzur, C.; Xiao, C.; Bourgeois, L.; Zhang, X.; MacFarlane, D. R. Nanostructured photoelectrochemical solar cell for nitrogen reduction using plasmon-enhanced black silicon. *Nature Communications* **2016**, *7*, 11335.

86. Montoya, J. H.; Tsai, C.; Vojvodic, A.; Nørskov, J. K. The challenge of electrochemical ammonia synthesis: A new perspective on the role of nitrogen scaling relations. *ChemSusChem* **2015**, *8*, 2180–2186.
87. Singh, A. R.; Rohr, B. A.; Schwalbe, J. A.; Cargnello, M.; Chan, K.; Jaramillo, T. F.; Chorkendorff, I.; Nørskov, J. K. Electrochemical Ammonia Synthesis-The Selectivity Challenge. *ACS Catal.* **2017**, *7*, 706–709.
88. Emmett, P. H.; Brunauer, S. THE ADSORPTION OF NITROGEN BY IRON SYNTHETIC AMMONIA CATALYSTS. *Journal of the American Chemical Society* **1933**, *55*, 1738–1739.
89. Ertl, G.; Grunze, M.; Weiss, M. Chemisorption of N₂ on an Fe(100) surface. *Journal of Vacuum Science and Technology* **1976**, *13*, 314–317.
90. Spencer, N. D.; Schoonmaker, R. C.; Somorjai, G. A. Structure sensitivity in the iron single-crystal catalysed synthesis of ammonia. *Nature* **1981**, *294*, 643–644.
91. Honkala, K. Ammonia Synthesis from First-Principles Calculations. *Science* **2005**, *307*, 555–558.
92. Vojvodic, A.; Medford, A. J.; Studt, F.; Abild-Pedersen, F.; Khan, T. S.; Bligaard, T.; Nørskov, J. K. Exploring the limits: A low-pressure, low-temperature Haber-Bosch process. *Chemical Physics Letters* **2014**, *598*, 108–112.
93. Karlberg, G. S.; Rossmeisl, J.; Nørskov, J. K. Estimations of electric field effects on the oxygen reduction reaction based on the density functional theory. *Physical Chemistry Chemical Physics* **2007**, *9*, 5158.
94. He, Z.-D.; Hanselman, S.; Chen, Y.-X.; Koper, M. T. M.; Calle-Vallejo, F. Importance of Solvation for the Accurate Prediction of Oxygen Reduction Activities of Pt-Based Electrocatalysts. *The Journal of Physical Chemistry Letters* **2017**, *8*, 2243–2246.

95. van der Ham, C. J. M.; Koper, M. T. M.; Hetterscheid, D. G. H. Challenges in reduction of dinitrogen by proton and electron transfer. *Chem. Soc. Rev.* **2014**, *43*, 5183.
96. Abghoui, Y.; Garden, A. L.; Howalt, J. G.; Vegge, T.; Skúlason, E. Electroreduction of N₂ to Ammonia at Ambient Conditions on Mononitrides of Zr, Nb, Cr, and V: A DFT Guide for Experiments. *ACS Catalysis* **2016**, *6*, 635–646.
97. Yates, J. T.; Szabó, A.; Henderson, M. A. *Structure-Activity and Selectivity Relationships in Heterogeneous Catalysis, Proceedings of the ACS Symposium on Structure-Activity Relationships in Heterogeneous Catalysis*; Elsevier, 1991; pp 273–290.
98. McFarland, E. W.; Metiu, H. Catalysis by Doped Oxides. *Chemical Reviews* **2013**, *113*, 4391–4427.
99. Hobiger, G.; Herzig, P.; Eibler, R.; Schlapansky, F.; Neckel, A. The influence of titanium and oxygen vacancies on the chemical bonding in titanium oxide. *Journal of Physics: Condensed Matter* **1990**, *2*, 4595–4612.
100. Goldsmith, B. R.; Sanderson, E. D.; Bean, D.; Peters, B. Isolated catalyst sites on amorphous supports: A systematic algorithm for understanding heterogeneities in structure and reactivity. *The Journal of Chemical Physics* **2013**, *138*, 204105.
101. Kobwittaya, K.; Sirivithayapakorn, S. Photocatalytic reduction of nitrate over TiO₂ and Ag-modified TiO₂. *Journal of Saudi Chemical Society* **2014**, *18*, 291–298.
102. Kominami, H.; Gekko, H.; Hashimoto, K. Photocatalytic disproportionation of nitrite to dinitrogen and nitrate in an aqueous suspension of metal-loaded titanium(IV) oxide nanoparticles. *Physical Chemistry Chemical Physics* **2010**, *12*, 15423.
103. Ranjit, K.; Viswanathan, B. Photocatalytic reduction of nitrite and nitrate ions to ammonia on M/TiO₂ catalysts. *Journal of Photochemistry and Photobiology A: Chemistry* **1997**, *108*, 73–78.

104. Shand, M.; Anderson, J. A. Aqueous phase photocatalytic nitrate destruction using titania based materials: routes to enhanced performance and prospects for visible light activation. *Catalysis Science & Technology* **2013**, *3*, 879.
105. Xie, X.-Y.; Wang, Q.; Fang, W.-H.; Cui, G. DFT Study on Reaction Mechanism of Nitric Oxide to Ammonia and Water on a Hydroxylated Rutile TiO₂(110) Surface. *The Journal of Physical Chemistry C* **2017**, *121*, 16373–16380.
106. Lozovskii, A. V.; Stolyarova, I. V.; Prikhod'ko, R. V.; Goncharuk, V. V. Research of photocatalytic activity of the Ag/TiO₂ catalysts in the reduction reaction of nitrate-ions in aqueous media. *Journal of Water Chemistry and Technology* **2009**, *31*, 360–366.
107. Pollema, C. H.; Milosavljević, E. B.; Hendrix, J. L.; Solujić, L.; Nelson, J. H. Photocatalytic oxidation of aqueous ammonia (ammonium ion) to nitrite or nitrate at TiO₂ particles. *Monatshefte fr Chemie Chemical Monthly* **1992**, *123*, 333–339.
108. Wang, A.; Edwards, J. G.; Davies, J. A. Photooxidation of aqueous ammonia with titania-based heterogeneous catalysts. *Solar Energy* **1994**, *52*, 459–466.
109. Kominami, H.; Kitsui, K.; Ishiyama, Y.; Hashimoto, K. Simultaneous removal of nitrite and ammonia as dinitrogen in aqueous suspensions of a titanium(iv) oxide photocatalyst under reagent-free and metal-free conditions at room temperature. *RSC Adv.* **2014**, *4*, 51576–51579.
110. Urabe, K. Isotopic equilibration of nitrogen on potassium-promoted transition metal catalysts. *Journal of Catalysis* **1978**, *54*, 436–438.
111. Giannozzi, P. et al. QUANTUM ESPRESSO: a modular and open-source software project for quantum simulations of materials. *Journal of Physics: Condensed Matter* **2009**, *21*, 395502 (19pp).

112. Bahn, S. R.; Jacobsen, K. W. An object-oriented scripting interface to a legacy electronic structure code. *Comput. Sci. Eng.* **2002**, *4*, 56–66.
113. Monkhorst, H. J.; Pack, J. D. Special points for Brillouin-zone integrations. *Physical Review B* **1976**, *13*, 5188–5192.
114. Bengtsson, L. Dipole correction for surface supercell calculations. *Physical Review B* **1999**, *59*, 12301–12304.
115. Bredow, T.; Giordano, L.; Cinquini, F.; Pacchioni, G. Electronic properties of rutile TiO₂ ultrathin films: Odd-even oscillations with the number of layers. *Physical Review B - Condensed Matter and Materials Physics* **2004**, *70*, 1–6.
116. Patel, M.; Sanches, F. F.; Mallia, G.; Harrison, N. M. A quantum mechanical study of water adsorption on the (110) surfaces of rutile SnO₂ and TiO₂: investigating the effects of intermolecular interactions using hybrid-exchange density functional theory. *Phys. Chem. Chem. Phys.* **2014**, *16*, 21002–21015.
117. Wellendorff, J.; Silbaugh, T. L.; Garcia-Pintos, D.; Nørskov, J. K.; Bligaard, T.; Studt, F.; Campbell, C. T. A benchmark database for adsorption bond energies to transition metal surfaces and comparison to selected DFT functionals. *Surface Science* **2015**, *640*, 36–44.
118. Li, W.-K.; Gong, X.-Q.; Lu, G.; Selloni, A. Different Reactivities of TiO₂ Polymorphs: Comparative DFT Calculations of Water and Formic Acid Adsorption at Anatase and Brookite TiO₂ Surfaces. *J. Phys. Chem. C* **2008**, *112*, 6594–6596.
119. Zheng, T.; Wu, C.; Chen, M.; Zhang, Y.; Cummings, P. T. A DFT study of water adsorption on rutile TiO₂ (110) surface: The effects of surface steps. *The Journal of Chemical Physics* **2016**, *145*, 044702.

120. Morgan, B. J.; Watson, G. W. A DFT+U description of oxygen vacancies at the TiO₂ rutile (110) surface. *Surface Science* **2007**, *601*, 5034–5041.
121. Landmann, M.; Rauls, E.; Schmidt, W. G. The electronic structure and optical response of rutile, anatase and brookite TiO₂. *Journal of Physics: Condensed Matter* **2012**, *24*, 195503.
122. Deák, P.; Aradi, B.; Frauenheim, T. Polaronic effects in TiO₂ calculated by the HSE06 hybrid functional: Dopant passivation by carrier self-trapping. *Phys. Rev. B* **2011**, *83*.
123. Jauho, T. S.; Olsen, T.; Bligaard, T.; Thygesen, K. S. Improved description of metal oxide stability: Beyond the random phase approximation with renormalized kernels. *Phys. Rev. B* **2015**, *92*.
124. Walker, E.; Ammal, S. C.; Terejanu, G. A.; Heyden, A. Uncertainty Quantification Framework Applied to the Water–Gas Shift Reaction over Pt-Based Catalysts. *The Journal of Physical Chemistry C* **2016**, *120*, 10328–10339.
125. Medford, A. J.; Vojvodic, A.; Hummelshøj, J. S.; Voss, J.; Abild-Pedersen, F.; Studt, F.; Bligaard, T.; Nilsson, A.; Nørskov, J. K. From the Sabatier principle to a predictive theory of transition-metal heterogeneous catalysis. *Journal of Catalysis* **2015**, *328*, 36–42.
126. Nozik, A. J.; Memming, R. Physical Chemistry of Semiconductor-Liquid Interfaces. *The Journal of Physical Chemistry* **1996**, *100*, 13061–13078.
127. Scanlon, D. O.; Dunnill, C. W.; Buckeridge, J.; Shevlin, S. A.; Logsdail, A. J.; Woodley, S. M.; Catlow, C. R. A.; Powell, M. J.; Palgrave, R. G.; Parkin, I. P.; Watson, G. W.; Keal, T. W.; Sherwood, P.; Walsh, A.; Sokol, A. A. Band alignment of rutile and anatase TiO₂. *Nature Materials* **2013**, *12*, 798–801.